Chemistry–A European Journal
Research Article
doi.org/10.1002/chem.202303067
Chemistry Europe
European Chemical Societies Publishing
www.chemeurj.org

Revealing the Origin of Fast Delayed Fluorescence in a Donor Functionalized Bisterpyridine

Felix D. Goll,[a] Andreas Schelhorn,[a] Džiugas Litvinas,[b] Francisco Tenopala-Carmona,[b] Lev Kazak,[c] Fedor Jelezko,[c] Christoph Lambert,[d] Malte C. Gather,[b, e] Alexander J. C. Kuehne,[a] and Ulrich Ziener*[a]

A new carbazole-substituted bisterpyridine with pronounced delayed fluorescence is presented. While the molecular donor-acceptor-donor design suggests the origin of this to be thermally activated delayed fluorescence (TADF), results from various photophysical characterizations, OLED characteristics, temperature-dependent NMR spectroscopy, and DFT calculations all point against the involvement of triplet states. The molecule exhibits blue emission at about 440 nm with two or more fast decay channels in the lower nanosecond range in both solution and thin films. The delayed emission is proposed to be caused by rotational vibrational modes. We suggest that these results are generally applicable, especially for more complex molecules, and should be considered as alternative or competitive emissive relaxation pathways in the field of organic light emitting materials.

Introduction

Organic molecules with delocalized π-systems and in particular donor-acceptor-systems linked by a π bridge are of special interest, due to their modularity in composition and their special properties.[1] Such donor-acceptor compounds have found application in various fields, from emitters with thermally activated delayed fluorescence (TADF)[2] to bioimaging probes[3] and photocatalysts.[4,5] In classical TADF emitters, the donor and acceptor moieties are twisted towards one another leading to a minimization in the energy gap ΔE_{ST} between triplet and emissive singlet state.[6] Triplet states can thus be converted into excited singlet states via reverse intersystem crossing (RISC). This way, triplet states can contribute to fluorescence and are not lost through thermal relaxation.[7] Typical characteristics of TADF include (i) the presence of a multiexponential decay, (ii) temperature dependence of the delayed component, and (iii) an external quantum efficiency EQE beyond the spin statistical limit of 0.25 (1 emissive singlet versus 3 dark triplets in conventional emitters).[7] This mechanistic understanding has led to the development of new materials with similar pathways that can also be exploited for TADF; for example, hot exciton pathways, where extremely fast RISC occurs not from the T_1 to the S_1, but among higher lying triplet and singlet states.[8] In addition, TADF is not limited to covalently linked, twisted donor-acceptor systems, but exciplexes formed by donor and acceptor molecules also show TADF.[9,10] A variety of powerful exciplexes have been developed based on pyrimidine-containing bisdipyridinylphenyl and bisterpyridine acceptors.[9,10] The structural variety of these pyrimidine-centered oligopyridine isomers enables precise tuning of the acceptor strength as well as designing the steric and electronic constraints during complex formation with an electron donor molecule. This donor molecule is typically based on carbazole and the most prominent candidate for exciplex formation is tris(*N*-carbazol)-triphenylamine (TCTA). While several donor-acceptor combinations display TADF behaviour in covalently connected twisted configuration as well as in exciplexes,[11,12] oligopyridine compounds have not been covalently connected to a donor moiety for TADF emission. Both exciplex and covalently connected donor-acceptor systems entail a charge transfer (CT) excited state, for which the emission is bathochromically shifted compared with the fluorescence of the individual donor and acceptor units. In exciplexes specifically, the face-to-face association of donor and acceptor molecules leads to steric constraints, which will limit rotational and vibrational degrees of freedom. To this point, there are no steric constraints that

[a] F. D. Goll, A. Schelhorn, Prof. Dr. A. J. C. Kuehne, Prof. Dr. U. Ziener
Institute of Organic Chemistry III –
Macromolecular Chemistry and Organic Materials
Ulm University
89081 Ulm (Germany)
E-mail: ulrich.ziener@uni-ulm.de
[b] D. Litvinas, Dr. F. Tenopala-Carmona, Prof. Dr. M. C. Gather
Humboldt Centre for Nano- and Biophotonics
Department of Chemistry
Greinstraße 4–6, 50939 Köln (Germany)
[c] L. Kazak, Prof. Dr. F. Jelezko
Institute for Quantum Optics
Ulm University
89081 Ulm (Germany)
[d] Prof. Dr. C. Lambert
Institut für Organische Chemie
Julius-Maximilians-Universität Würzburg
Am Hubland, 97074 Würzburg (Germany)
[e] Prof. Dr. M. C. Gather
SUPA, School of Physics and Astronomy
University of St Andrews
North Haugh, KY16 9SS St Andrews, Fife, (UK)

Supporting information for this article is available on the WWW under https://doi.org/10.1002/chem.202303067

will limit vibrational or rotational degrees of freedom in the aforementioned covalently connected donor-acceptor moieties.

However, to date, such donor-acceptor molecules have not been synthesized and the exact nature of the emission process in the molecules has not been elucidated. Investigation of these unexplored material classes could give insight into limitations in size for covalently connected donor-acceptor systems for TADF and might also elucidate alternative relaxation pathways, which could be mistaken as TADF. Based on the finding that exciplexes based on bisterpyridines[13] and TCTA show TADF behaviour with significant triplet contribution,[10] we have designed a corresponding covalently donor-functionalized biscarbazolylbis(bipyridine) Cz_2BBP (**4**) (see Scheme 1). The emission lifetime of the molecule indeed displays two short components with *identical* emission spectra. The molecule fulfils all the criteria usually invoked for TADF, but it is shown that it does not have triplet participation, but two energetically degenerate rotamers, which are proposed to be the cause of the observed effects.

Results and Discussion

Synthesis

The synthesis of the donor functionalized bisterpyridine Cz_2BBP (**4**) is started from readily available precursors in analogy to procedures described in the literature (see Scheme 1).[13–16] The palladium catalysed cross-coupling reaction between *p*-bromobenzaldehyde and carbazole furnishes 4-(9H-carbazol-9-yl)benzaldehyde in quantitative yield. The subsequent aldol condensation produces the chalcone **2** in good yields. In this step, temperature control is of utmost importance, as the product easily decomposes at elevated temperatures. The same applies for the subsequent double Kröhnke reaction. Product **4** precipitates from the reaction solution and is purified by sublimation. The yield of this final step ranges from 30 to 40%.

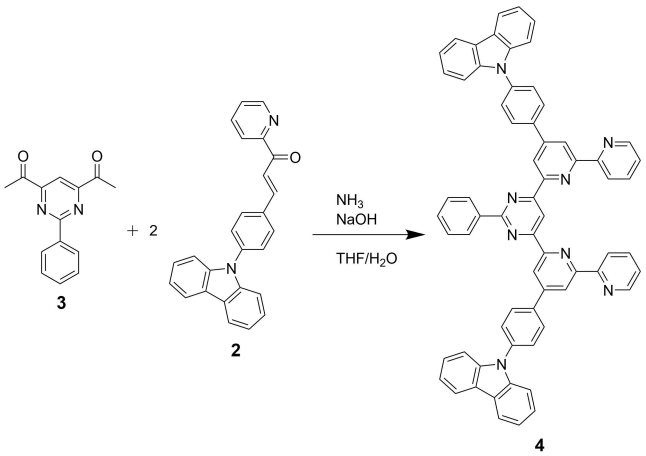

Scheme 1. Synthesis of Cz_2BBP (**4**) from diketone **3** and chalcone **2** in a Kröhnke pyridine synthesis.

Photophysical Characterization

Our initial spectroscopic characterization of the newly synthesized Cz_2BBP (**4**) delivers the energies for the $S_1 \leftarrow S_0$ transition with 3.41 eV and for the $S_1 \rightarrow S_0$ relaxation with 3.32 eV, as shown in Figure 1. The transition energies are calculated from the onsets of the respective peaks. In addition to toluene (normalized solvent polarity parameter $E_T^N = 0.099$),[17] absorption and emission spectra are also recorded using more polar aromatic solvents, namely anisole ($E_T^N = 0.198$) and benzonitrile ($E_T^N = 0.333$). The fluorescence is evidently strongly solvatochromic, which indicates a CT S_1 excited state. From fluorescence and phosphorescence measurements at −196 °C in toluene the $T_1 \rightarrow S_0$ transition is determined to be 2.79 eV and with an $S_1 \rightarrow S_0$ transition energy of 3.32 eV the S_1–T_1 energy gap ΔE_{ST} can be determined to be 0.53 eV (see Figure S7 in the Supporting Information). The quantum yield ϕ is 58% at room temperature. Fluorescence lifetimes could be fitted best using a biexponential model, delivering photoluminescence lifetimes of $\tau_1 = 2.0$ ns and $\tau_2 = 3.7$ ns, as shown in Figure 4 (pink curve). While the first component can be easily attributed to prompt fluorescence from the S_1 state, the origin of the second relatively short lifetime remains unclear. Several possible explanations can be considered: (i) TADF emission mediated by the covalent but twisted donor-acceptor sequence,[7] (ii) competing emission from an impurity[18] or (iii) the presence of different conformational isomers[19] could lead to the observed delayed emission.

The presence of impurities can be ruled out since the material was carefully purified, ultimately by repeated sublimation.

The photoluminescence lifetimes τ as well as quantum yields ϕ are found to be affected by the presence of oxygen, which supports the involvement of triplet states in the excited state relaxation pathway. Ground state triplet oxygen can quench excited triplet states in emitters.[20]

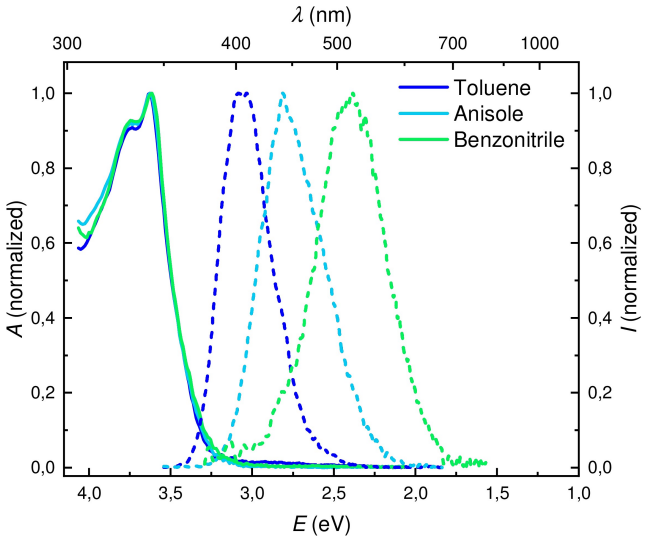

Figure 1. Absorbance and photoluminescence spectra of Cz_2BBP (**4**) in different solvents, absorbance spectra in solid lines, photoluminescence spectra in dashed lines.

For classical TADF with a small energy gap $\Delta E_{ST} \approx 0$ *eV*, the lifetimes of the delayed component are usually much longer in the microsecond range than our observed τ_2. In the case of hot exciton mediated TADF, shorter lifetimes are observed, in the range of a few hundred nanoseconds[8] and for hot exciplexes even down to a few nanoseconds.[21] These hot mechanisms are based on fast RISC from higher excited triplet states T_n with $n > 1$. To prevent internal conversion (IC) from these higher states within the triplet manifold, a large energy gap between T_1 and T_2 of around 1 eV is required.

The condition for classical TADF is hardly fulfilled for Cz_2BBP (**4**) with $\Delta E_{ST} = 0.53$ *eV*. Thus, this possibility can be excluded due to the observed delayed lifetime in the nanosecond range but a "hot mechanism" shall be still considered. To gain further insight into the energies of relevant states, DFT calculations are carried out.

DFT Calculations

To get better insight into the electronic structure of Cz_2BBP (**4**), we perform time-dependent density functional theory (TD-DFT). The geometry optimization is done using the hybrid B3LYP functional and 6-31 + G(d) basis set and TD-DFT using the long-range corrected LC-ωPBE functional also with 6-31 + G(d) (see Figure 2).

As is typical for DFT, the absolute energies of S_1 and T_1 states are slightly overestimated compared to the measured values of fluorescence and phosphorescence onsets (3.32 eV experimentally versus 3.65 eV calculated for S_1 and 2.79 eV versus 3.22 eV, respectively, for T_1) (compare Figure 1 and Figure S7 with Figure 2). However, the energy differences ΔE between different states are in good agreement with the experimentally determined values. This can be seen from the ΔE_{ST} of 0.42 eV (exp. 0.53 eV) and the S_1-S_2 energy difference of 0.28 eV (exp. 0.36 eV). The latter can be estimated from transient absorption spectra (see Figure S10 in the Supporting Information). The semiquantitative results of the calculation are therefore used to explain the observed phenomena: the ΔE_{ST} gap is too large to enable classical TADF, which appears to be in agreement with the short τ_2 lifetime of the delayed component. There are several triplet states energetically close to the S_1 state, with T_{10} almost degenerate with S_1, which could in principle allow for hot exciton TADF.[8] However, the large number of close lying triplet states with narrow energetic spacing of typically less than 0.2 eV suggests that IC within the triplet manifold would be much faster than RISC to the singlet manifold. As a result, we would expect excited triplet states to relax to T_1 and the origin of the short τ_2 remains unclear. To rule out or confirm triplet participation and RISC during the emission process, we process the emitter into thin films with the intention to characterize the electroluminescence of Cz_2BBP (**4**).

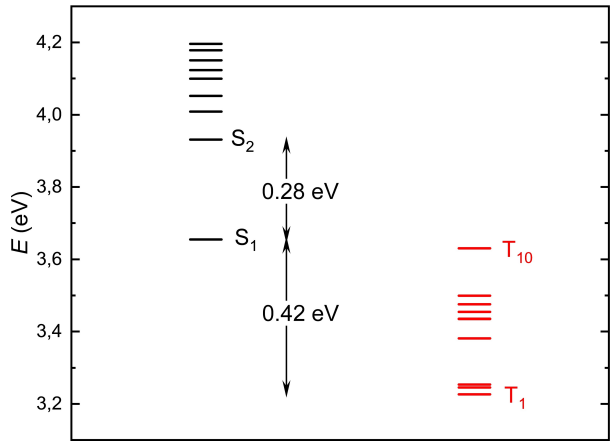

Figure 2. Calculated energetic states of Cz_2BBP (**4**) in the excited state, singlets in black, triplets in red. Energies relative to the S_0 state.

Thin Film Characterization

We co-deposit Cz_2BBP (**4**) in a matrix of 3,3′-di(9H-carbazol-9-yl)-1,1′-biphenyl (mCBP) as the host material using vacuum deposition. The thin films are used to determine the optical constants, photoluminescence quantum yield in the solid ϕ_s and emitter transition dipole moment (TDM) orientation (see Figures S13 to S16). The photoluminescence spectrum peak remains approximately constant with increasing doping fraction of **4** ($\lambda_{em} \approx 421$–422 nm), as does the width of the spectrum (FWHM ≈ 60 nm) (see Figure S14). The corresponding ϕ_s increases from 47.5 to 51.8 % for doping levels of 10 to 20 wt.%. A slight anisotropy in the optical constants of the films is determined from variable-angle spectroscopic ellipsometry, as can be seen in Figure S15. This anisotropy is stronger for the 20 wt.% sample indicating a slightly favoured in-plane orientation of the emitter TDMs. The latter result is further substantiated by angle-resolved photoluminescence (ARPL) measurements (Figure S16).[22] Fitting the ARPL data by an optical model of oriented emitting dipoles[23] yields TDM orientations with anisotropy factors $a = 0.29$ and $a = 0.25$, corresponding to 71 % and 75 % of horizontal emissive dipoles in the 10 wt.% and 20 wt.% films, respectively.

OLED

We carry on to produce multilayered OLED stacks of the following sequence: indium tin oxide (ITO) (100 nm)/molybdenum oxide MoO_3 (1 nm)/1,1-bis[(di-4-tolylamino)phenyl]cyclohexane (TAPC) (25 nm)/1,3-bis(N-carbazolyl)benzene (mCP) (10 nm)/mCBP:Cz_2BBP (**4**) (30 nm)/1,3,5-tris(m-pyridin-3-ylphenyl)benzene (TmPyPB) (35–50 nm)/lithium fluoride (LiF) (1 nm)/aluminium (Al) (100 nm), with TAPC as the hole transport layer (HTL), mCP as the electron blocking layer (EBL) and TmPyPB as the electron transport layer (ETL) (see Figure 3a). Electroluminescence characterization is performed using the in-house setup.[22] We again investigate 10 wt.% and 20 wt.% of Cz_2BBP (**4**) in mCBP matrix as the emissive layer.

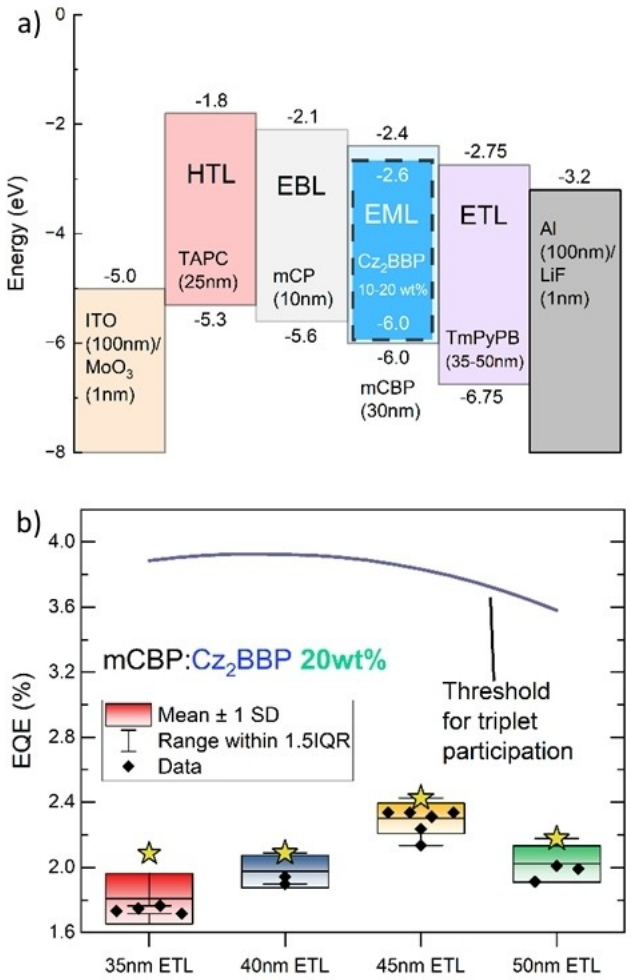

Figure 3. (a) Fabricated OLED stack energy level diagram. (b) Experimental EQE value distributions across different ETL thicknesses for fabricated OLEDs with an EML of mCBP:Cz_2BBP (**4**) 20 wt.%. Champion devices are shown with the star icon. The solid curve corresponds to the simulated maximum EQE for a fluorescent OLED (i.e. no triplet emission) with the corresponding cavity design and ETL thickness, assuming an EMZ (emission zone) profile interpolated from the fitted distributions shown in Figure S18b.

Compared to the photoluminescence in thin films, the electroluminescence spectrum is redshifted ($\lambda_{peak,EL}$ = 427 nm) and broadened (FWHM = 71–73 nm), due to cavity effects of the OLED stack (see Figures S17 and S18). As the ETL thickness increased from 35 to 50, the CIE (Commission Internationale de l'Éclairage) color coordinates shift from [0.157, 0.075] to [0.156, 0.058] for 10 wt.%, and [0.156, 0.067] to [0.152, 0.052] for 20 wt.% of Cz_2BBP (**4**) in mCBP. Maximum experimental luminance and EQE is achieved for 45 nm ETLs: 1130 cd/m^2, 1.94 ± 0.09% and 595 cd/m^2, 2.30 ± 0.09% for 10 wt.% and 20 wt.% devices, respectively. To assess the triplet participation in these devices, a threshold external quantum efficiency value EQE_t is determined from the experimental ϕ_s = 51.8%, optical cavity simulations[23] for the outcoupling efficiency η_{out}, as well as assuming a charge balance factor $\gamma = 1$ (i.e. assuming the ideal case of equilibrated holes and electrons) and a singlet/triplet contribution $\eta_{S/T}$ (= 0.25 for pure fluorescence emitters).[22] More detailed information of evaluating the EQE_t is presented in the Supporting Information. If the experimental EQE_e for optimized devices lies below EQE_t, the emission occurs as pure fluorescence without TADF contribution. Figure 3b shows the results for content and four different ETL layer thicknesses. The OLED device with 20 wt.% Cz_2BBP (**4**) emitter in mCBP matrix exhibits EQE_e in the range between 1.6 and 2.4%, which is well below the corresponding EQE_t (between 3.5 and 3.9%) indicating fluorescence and absence of TADF. Corresponding results are obtained for the 10 wt.% Cz_2BBP (**4**) OLED (see Figure S21).

Temperature-Dependent Photoluminescence Decay Measurements

According to time dependent fluorescence spectra, both temporally separated components of the emission are of the same wavelength. Having ruled out triplet participation in the emission process, the delayed component of the fluorescence would require two distinct excited singlet states of similar energy difference to the ground state with different transition probabilities to the ground state. To further elucidate the proposed states, temperature controlled TCSPC measurements are performed in anisole and toluene (full datasets are shown in Figures S8 and S9 in the Supporting Information). Selected decay curves including fits, following the general equation $y = y_0 + A_1{}^*e^{-\frac{x}{\tau_1}} + A_2{}^*e^{-\frac{x}{\tau_2}}$ with biexponential character increasing with temperature, can be seen in Figure 4. In addition, the ϕ in both solvents has been determined as a function of temperature. For all temperatures the curves can be adequately fitted only by a biexponential decay as in the case of room temperature.

The measurements in anisole show a clear temperature dependent trend: the lifetime of the short component τ_1 is approximately temperature-independent, while the longer component decreases in lifetime τ_2 with increasing temperature, as visible in Figure 5.

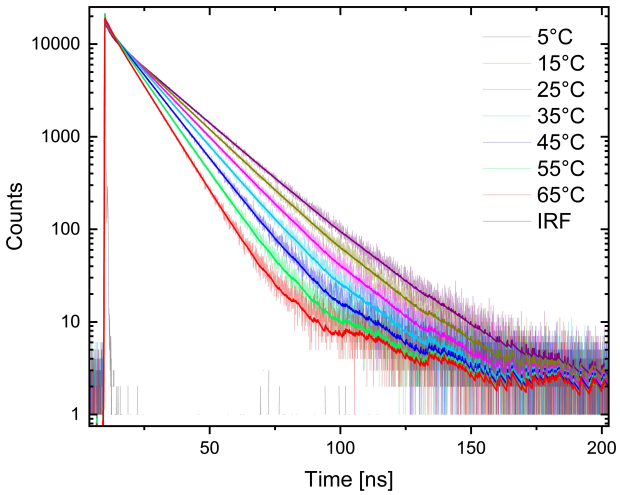

Figure 4. Fluorescence decay curves of Cz_2BBP (**4**) in anisole at various temperatures. Some curves were omitted for clarity.

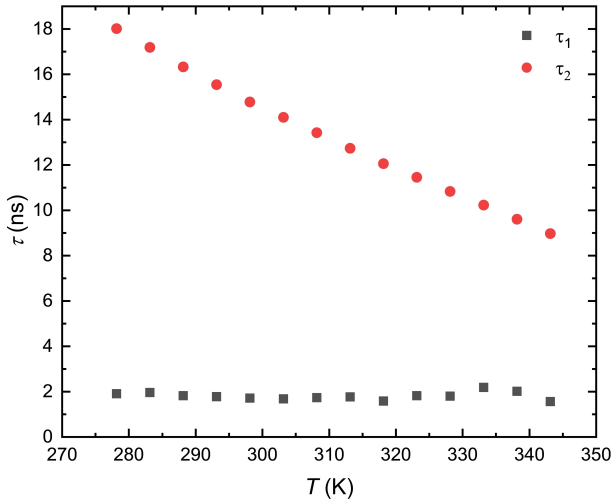

Figure 5. Temperature dependence of fluorescence lifetimes of Cz_2BBP (**4**) in anisole solution.

Additionally, the pre-exponential factor of the longer component A_2 increases with temperature. To explain this observation, we propose the presence of two rotamers with isoenergetic S_1 and S_1' states, whose interconversion rates are influenced by temperature. Decay time τ_1 is caused by prompt fluorescence, while τ_2 is caused by the isomerisation, as shown in Figure 6.

We assume that the reason for the formation of two rotamers is the relatively large energy barrier for the rotation around the carbazole-phenyl bond. With this assumption, the activation energy of the isomerization can be calculated using a simple Arrhenius approach. The isomerization lifetime τ_{iso} is calculated from the difference of τ_1 and τ_2, and the rate constants are calculated as the reciprocal lifetimes in turn. The relationship between the viscosity of a solution and the fluorescence properties of the emitter dissolved in it is well known in the literature.[24,25] These correlations were used to correct the measured lifetimes for the temperature-dependent viscosity of toluene and anisole using the Stokes-Einstein equation (see Supporting Information). For this purpose, the coefficient of viscosity and temperature has been normalised to the lowest temperature of the series and included as a correction factor in the following data points (see Supporting Information). As states S_1 and S_1' are degenerate, excitation from S_0 can lead to population of either one and in turn the emission can originate from both states. However, when the excited state is isomerized by rotation, a delay of the emission will occur. Since the geometry of the molecule is not significantly changed by the excitation, as determined by our DFT calculations, the ground state will also feature an isoenergetic pair of two rotamers. The evaluation of the data measured in anisole yields an activation energy of $\Delta E_a = 6.42 \pm 0.37$ kJ/mol, as can be seen in Figure 7.

Thus, the energy is in a range comparable to literature (ca. 4 kJ/mol)[26] for the rotation barrier between 3,6-di-*tert*-butylcarbazole and a functionalized phenyl linker. In toluene solution, the Arrhenius plot shows a more complicated behaviour, with two slopes and a transitional area located around room temperature. At temperatures below room temperature, once again a negative slope can be fitted, yielding an activation energy of $\Delta E_a = 4.38 \pm 1.04$ kJ/mol, again comparable both to the value in anisole and to literature. The slightly larger activation barrier in anisole can be attributed to a stronger interaction of the fluorophore with the more polar solvent molecules. From literature, it is evident that the rotation around the Ph–Cz bond cannot cross the phenyl plane as the energy required for that was calculated to be around 140 kJ/mol.[26] However, there are two local energetic minima around dihedral angles of 60°, which corresponds to the performed geometry optimization calculations, yielding an angle of 58° in the equilibrated state. It is therefore assumed that the carbazole performs a rocking motion between 58° and 122° relative to the phenyl plane (see Figure 8).

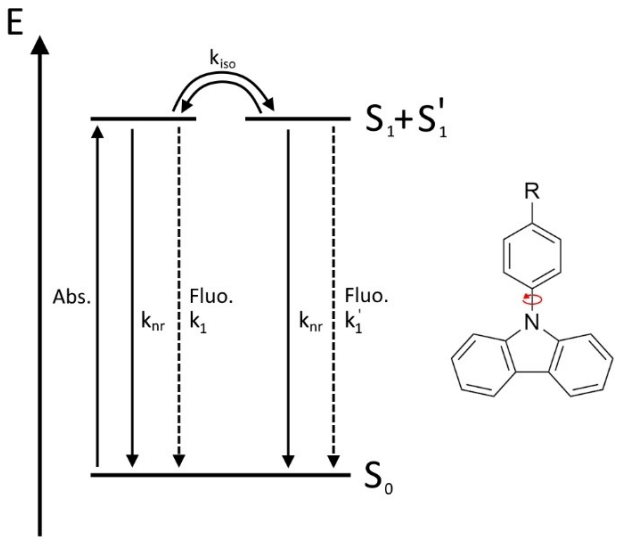

Figure 6. Schematic depiction of the rotamer isomerization in the excited state. S_1 and S_1' are degenerate and therefore interchangeable.

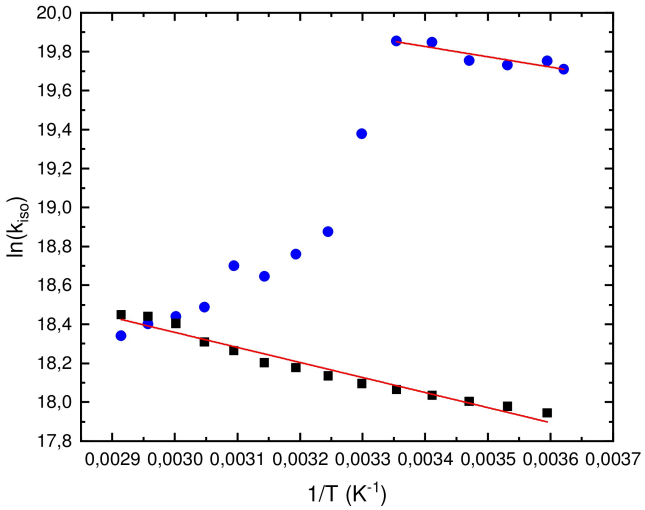

Figure 7. Arrhenius plots of Cz_2BBP (**4**) in toluene (blue) and anisole (black) solution with linear fits (red).

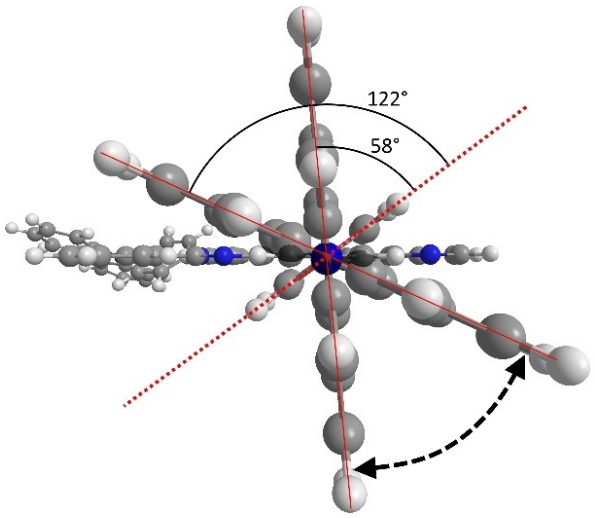

Figure 8. Two local energetic minima of the carbazole rotation as seen along the Cz–Ph bond. The bulk of the molecule in the horizontal plane, the phenyl bridge marked with a dotted red line and the two possible rotamers marked with solid red lines.

The behaviour above room temperature is obviously more complicated and would indicate a negative activation energy. Thus, this model is probably not suitable for explaining this area of the Arrhenius plot.

Supporting this, in toluene ϕ decreases quickly with rising temperature, while in anisole ϕ is constant over the entire temperature range. This can in part be explained by the different trends of viscosity γ in both solvents: in anisole, the viscosity barely changes across the tested temperature range ($\gamma = 1.01$ mPa·s and 0.95 mPa·s), while in toluene it goes down from $\gamma = 0.73$ mPa·s to 0.34 mPa·s. A lower viscosity would naturally lead to faster molecular kinetics, more collisions and thus higher probability for non-radiative relaxation. A similar measurement has also been carried out in a thin film of pure Cz_2BBP (**4**) produced by drop casting. Because of different local environments and a lack of dynamics in solid films of emitters, multiple emission lifetimes are often seen in solid film samples. However, the respective proportions and lifetimes are invariable in terms of temperature within the limits of the measurement accuracy (as seen in Figure S11 in the Supporting Information). This supports the assumption that the temperature dependence of the described process is dependent on the dynamics, meaning in our case the strongly restricted or rotation in **4** in the mCBP matrix. We have also investigated **4** encapsulated in various host materials (see above) by TCSPC. As in the solution, several different emission times are observed with unchanged emission spectra. The width of the lifetime distribution increases with increased polarity of the host material and decreases with the doping concentration of the emitter, as seen in Figures S23–S25 in the Supporting Information. The different emission times can be explained by the different local environments of the emitter molecules and by the rotational transitions that can also be observed in the solution. By contrast, an increased polarity of the environment causes a stronger interaction between host and emitter, which leads to a broadening of the distribution of emission times.

NMR Measurements

To further substantiate the proposed molecular mechanism for the biexponential emission, temperature dependent ^{1}H nuclear magnetic resonance (NMR) measurements have been carried out. NMR has been established as a viable tool for rotamer analysis, even for quantitation of their respective populations.[27] Due to the non-availability of deuterated anisole and the easy accessibility of the relevant temperature range in which the molecules show a similar behaviour in toluene as in anisole (below room temperature), these measurements are exclusively performed in toluene-d_8. All spectra have been calibrated using the chemical shift of added TMS, which has a well-known temperature dependence.[28] The resulting spectra are plotted with the spectrum measured at the lowest temperature ($T = 233$ K) at the bottom and the one with the highest temperature ($T = 313$ K) at the top, as shown in Figure 9.

In contrast to the two clearly different states visible from the TCSPC measurement, only one peak for each proton can be seen in the NMR spectra instead of two for both rotamers. This can be explained by the different time scales on which the measurements take place. While the NMR time scale is in the range of seconds, the lifetimes of the excitons are of the order

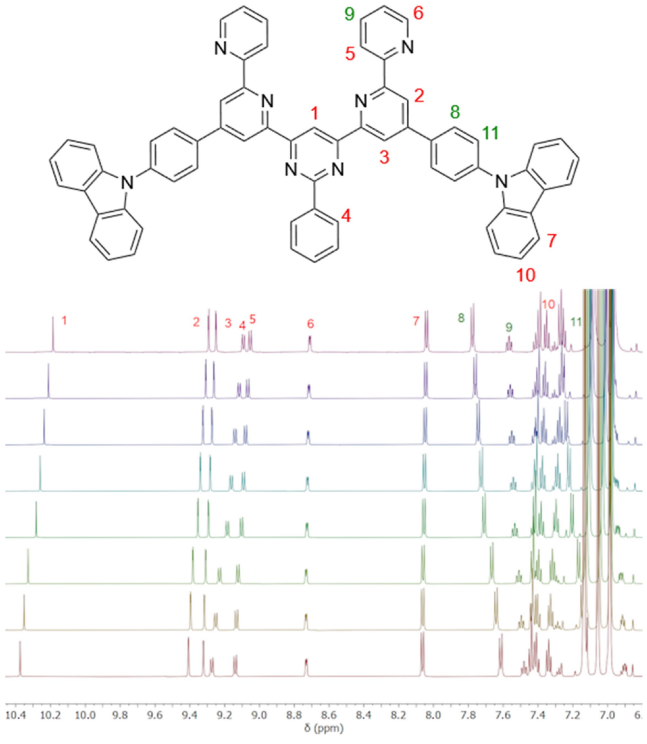

Figure 9. On top molecular formula of the characterized molecule with proton numbering corresponding to the labelled peaks in the spectra below. Protons with positive temperature shift marked in green, with negative temperature shift in red. On the bottom the stacked ^{1}H NMR spectra of Cz_2BBP (**4**) in toluene-d_8 at various temperatures, starting at 233 K at the bottom and rising to 313 K at the top.

of nanoseconds. This leads to an averaging of the signals in the NMR spectra. With H-H-correlation NMR spectroscopy all non-overlapping signals have been assigned to their respective protons. The resulting chemical shifts have been plotted against temperature, revealing that for all signals the chemical shift change follows a nearly linear trend. The proton chemical shifts are used as a proxy for the local electron density.[29] For most signals, the chemical shift decreases with increase in temperature, as can be seen in Figure 9. This behaviour is well-known and the temperature dependence of the proton chemical shifts can even be exploited for accurate determination of the temperature of the sample as shown in literature for methanol.[30] In that context the change in shift is explained by the weakening of H-bonds, with increasing temperature leading to increased electron density at said protons and thus stronger shielding. A similar explanation can be given for the oligopyridine, as the nitrogen atoms can form hydrogen bonds (C–H···N), too.[31] However, in contrast to the aforementioned literature study of methanol, there are intramolecular H bonds here. These bonds form between pyridine or pyrimidine rings and adjacent aromatic rings. Rising temperature would lead to an increase in the amplitude and frequency of the rotation around the bonds between neighbouring aromatic rings and therefore to decreased C–H···N bond efficiency. It is assumed that the decreased bonding strength, in turn, leads to stronger shielding of the involved protons. In the presented Cz_2BBP (**4**) molecule, the signal with the strongest temperature dependence in the upfield direction is the pyrimidine proton 1 (see Figure 9). This proton can form C–H···N bonds to two adjacent nitrogen atoms and thus experiences a rather strong change in shift with temperature increase. Besides this expected phenomenon for a few protons the opposite effect is seen, a downfield shift with rising temperature. This shift is most pronounced for protons 8 and 11, which are located at the phenyl linker between the neighbouring carbazole and pyridine units. These protons are expected to undergo the most severe electron loss with rising temperature as the donating effect of the carbazole is weakened by the greater amplitude of the Cz-phenyl-bond rotation.[32] This hypothesis is supported by the higher electron density at the carbazole moiety, due to the poorer conjugation at higher temperature, which is evident from the upfield shift of the carbazole protons. Since this part of the molecule is the only one in which two states separated by an energy barrier can exist as a result of rotation around a single bond, we propose that the two degenerate states described arise as a result of the Ph–Cz rotation.

Conclusions

In this work, the fluorescence emission of the donor-acceptor molecule Cz_2BBP (**4**) has been investigated. Two temporally separated but energetically identical events are found. These can presumably be assigned to two different rotamers separated by an energy barrier the size of which could be determined by means of temperature dependent TCSPC measurements. The obtained rotation barrier agrees with calculated values from the literature, whereby the analysis method used in this work, based on tempered TCSPC measurements, has not yet been described. For a more detailed elucidation of the nature of the rotamers involved, tempered ^{1}H NMR spectra have been recorded, and the temperature dependent chemical shifts determined. Based on the different trends of the signals of protons from different areas of the molecule, conclusions can be drawn about the aromatic rings involved in the rotation. Stronger rotation leads on the one hand to weaker C–H···N bonds and thus to a downfield shift of the protons involved, but on the other hand also to weaker conjugation between donor and acceptor regions and thus upfield shift of nearby protons. The presence of rotamers deduced from this is known from the literature but has so far only been predicted on the basis of calculations but demonstrated here with the help of experimental data. In principle, it seems likely that similar mechanisms may occur for many similar fluorophores especially with high degree of rotational freedom. The probability for such phenomena is likely to increase with the size of donor-acceptor molecules due to the rising number of degrees of freedom, which might contribute to potential relaxation pathways. If multiexponential emission curves are observed in the short time range, i.e. up to a few tens of nanoseconds, the presence of several conformational isomers should be considered.

Experimental Section

All experimental details (synthesis, optical measurements, thin film and OLED characterization) can be found in the Supporting Information to this article.

Supporting Information

The authors have cited additional references within the Supporting Information.[33–37]

Acknowledgements

Jun.-Prof. Dr. Andrea Pannwitz from the Institute of Inorganic Chemistry I at Ulm University is kindly acknowledged for giving us access to some spectrometers and Dr. Chang-Ki Moon from the Humboldt Centre for Nano- and Biophotonics for help with the ARPL and OLED optical modelling software based on his own work as described in [23]. This project has been partly funded by the European Union Horizon 2021 research and innovation programme under grant agreement No. 101073045 (TADFsolutions). M. C. G. acknowledges financial support by the Alexander von Humboldt Stiftung (Humboldt professorship). F. J. acknowledges support by BMBF and EU via QSens, H2020 ERC HyperQ project (856432), QCIRCLE (101059999, HORIZON), QuMicro (101046911, HORIZON), and FLORIN (101086142, HORIZON). Open Access funding enabled and organized by Projekt DEAL.

Conflict of Interests

The authors declare no conflict of interest.

Data Availability Statement

The data that support the findings of this study are available in the supplementary material of this article.

Keywords: donor-acceptor · fluorescence · isomerization · lifetime · oligopyridine

[1] F. Bureš, *RSC Adv.* **2014**, *4*, 58826–58851.
[2] H. Uoyama, K. Goushi, K. Shizu, H. Nomura, C. Adachi, *Nature* **2012**, *492*, 234–238.
[3] D. Li, Y. Xu, N. Zhou, J. Liu, R. Wang, T. Cheng, Y. Tang, W. Zhu, Y. Xu, X. Qian, *Dyes Pigm.* **2017**, *136*, 627–632.
[4] Q. A. Wu, F. Chen, C. C. Ren, X. F. Liu, H. Chen, L. X. Xu, X. C. Yu, S. P. Luo, *Org. Biomol. Chem.* **2020**, *18*, 3707–3716.
[5] J. Luo, J. Zhang, *ACS Catal.* **2016**, *6*, 873–877.
[6] L. S. Cui, H. Nomura, Y. Geng, J. U. k. Kim, H. Nakanotani, C. Adachi, *Angew. Chem. Int. Ed.* **2017**, *56*, 1571–1575.
[7] A. Monkman, in *Highly Effic. OLEDs*, Wiley-VCH Verlag GmbH & Co. KGaA, Weinheim, Germany, **2018**, pp. 425–463.
[8] Y. Xu, P. Xu, D. Hu, Y. Ma, *Chem. Soc. Rev.* **2021**, *50*, 1030–1069.
[9] K. H. Kim, S. J. Yoo, J. J. Kim, *Chem. Mater.* **2016**, *28*, 1936–1941.
[10] A. L. Schleper, S. Hillebrandt, C. Bannwarth, A. Mischok, S. Kwon, F. Buchner, F. Tenopala-Carmona, R. J. Behm, F. D. Goll, P. J. Welscher, M. Usselmann, U. Ziener, M. C. Gather, A. J. C. Kuehne, *J. Mater. Chem. C* **2022**, *10*, 7699–7706.
[11] X. Wei, T. Hu, Z. Li, Y. Liu, X. Hu, H. Gao, G. Liu, P. Wang, Y. Yi, Y. Wang, *Chem. Eng. J.* **2022**, *433*, 133546.
[12] M. Stanitska, M. Mahmoudi, N. Pokhodylo, R. Lytvyn, D. Volyniuk, A. Tomkeviciene, R. Keruckiene, M. Obushak, J. V. Grazulevicius, *J. Org. Chem.* **2022**, *87*, 4040–4050.
[13] U. Ziener, *J. Phys. Chem. B* **2008**, *112*, 14698–14717.
[14] D. Caterbow, U. Ziener, *Macroheterocycles* **2011**, *4*, 250–265.
[15] U. Ziener, J. Lehn, A. Mourran, M. Möller, *Chem. Eur. J.* **2002**, *8*, 951–957.
[16] C. Meier, U. Ziener, K. Landfester, P. Weihrich, *J. Phys. Chem. B* **2005**, *109*, 21015–21027.
[17] C. Reichardt, T. Welton, in *Empirical Parameters of Solvent Polarity*, Wiley-VCH Verlag GmbH & Co. KGaA, Weinheim, Germany, **2010**.
[18] C. Chen, Z. Chi, K. C. Chong, A. S. Batsanov, Z. Yang, Z. Mao, Z. Yang, B. Liu, *Nat. Mater.* **2021**, *20*, 175–180.
[19] L. Ji, S. Riese, A. Schmiedel, M. Holzapfel, M. Fest, J. Nitsch, B. F. E. Curchod, A. Friedrich, L. Wu, H. H. Al Mamari, S. Hammer, J. Pflaum, M. A. Fox, D. J. Tozer, M. Finze, C. Lambert, T. B. Marder, *Chem. Sci.* **2022**, *13*, 5205–5219.
[20] A. A. Abdel-Shafi, D. R. Worrall, *J. Photochem. Photobiol. A* **2005**, *172*, 170–179.
[21] A. L. Schleper, K. Goushi, C. Bannwarth, B. Haehnle, P. J. Welscher, C. Adachi, A. J. C. Kuehne, *Nat. Commun.* **2021**, *12*, 1–9.
[22] E. Archer, S. Hillebrandt, C. Keum, C. Murawski, J. Murawski, F. Tenopala-Carmona, M. C. Gather, *Adv. Opt. Mater.* **2021**, *9*, 2000838.
[23] C.-K. Moon, S.-Y. Kim, J.-H. Lee, J.-J. Kim, *Opt. Express* **2015**, *23*, A279.
[24] S. C. Lee, J. Heo, H. C. Woo, J. A. Lee, Y. H. Seo, C. L. Lee, S. Kim, O. P. Kwon, *Chem. A Eur. J.* **2018**, *24*, 13706–13718.
[25] M. A. Haidekker, E. A. Theodorakis, *Org. Biomol. Chem.* **2007**, *5*, 1669–1678.
[26] X. K. Chen, B. W. Bakr, M. Auffray, Y. Tsuchiya, C. D. Sherrill, C. Adachi, J. L. Bredas, *J. Phys. Chem. Lett.* **2019**, *10*, 3260–3268.
[27] M. Kraszni, Z. Szakács, B. Noszál, *Anal. Bioanal. Chem.* **2004**, *378*, 1449–1463.
[28] R. E. Hoffman, E. D. Becker, *J. Magn. Reson.* **2005**, *176*, 87–98.
[29] M. A. Everest, J. M. Vargason, *J. Chem. Educ.* **2013**, *90*, 926–929.
[30] N. Karschin, S. Krenek, D. Heyer, C. Griesinger, *Magn. Reson. Chem.* **2022**, *60*, 203–209.
[31] R. A. Pasternak, *Acta Crystallogr.* **1959**, *12*, 612–613.
[32] Y. Shi, H. Ma, Z. Sun, W. Zhao, G. Sun, Q. Peng, *Angew. Chem. Int. Ed.* **2022**, *61*, e202213463.
[33] G. E. Johnson, *J. Phys. Chem.* **1974**, *78*, 1512–1521.
[34] M. Furno, R. Meerheim, S. Hofmann, B. Lüssem, K. Leo, *Phys. Rev. B: Condens. Matter Mater. Phys.* **2012**, *85*, 1–21.
[35] D. Kelly, L. G. Franca, K. Stavrou, A. Danos, A. P. Monkman, *J. Phys. Chem. Lett.* **2022**, *13*, 6981–6986.
[36] N. Auerhammer, A. Schulz, A. Schmiedel, M. Holzapfel, J. Hoche, M. I. S. Röhr, R. Mitric, C. Lambert, *Phys. Chem. Chem. Phys.* **2019**, *21*, 9013–9025.
[37] N. Auerhammer, A. Schmiedel, M. Holzapfel, C. Lambert, *J. Phys. Chem. C* **2018**, *122*, 11720–11729.

Manuscript received: September 21, 2023
Accepted manuscript online: October 30, 2023
Version of record online: ■■, ■■

RESEARCH ARTICLE

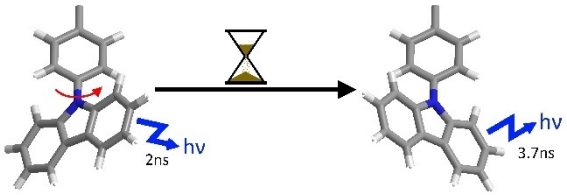

Two different, extremely short fluorescence lifetimes were found for a new carbazole-substituted bisbipyridine. Various methods, including tempered TCSPC, DFT and NMR spectroscopy were used to show the presence of two rotamers. These can transition into each other after optical excitation, causing two temporally different fluorescence events.

*F. D. Goll, A. Schelhorn, D. Litvinas, Dr. F. Tenopala-Carmona, L. Kazak, Prof. Dr. F. Jelezko, Prof. Dr. C. Lambert, Prof. Dr. M. C. Gather, Prof. Dr. A. J. C. Kuehne, Prof. Dr. U. Ziener**

1 – 9

Revealing the Origin of Fast Delayed Fluorescence in a Donor Functionalized Bisterpyridine